RGB-NIR IMAGING WITH EXPOSURE BRACKETING FOR JOINT DENOISING AND DEBLURRING OF LOW-LIGHT COLOR IMAGES

Hiroki Yamashita, Daisuke Sugimura and Takayuki Hamamoto

Graduate School of Engineering, Tokyo University of Science,
Katsushika-Ku, Tokyo, 125-8585, Japan

ABSTRACT

Color images taken in low light scenes are deteriorated with noise and motion blur. The simultaneous reduction of noise and motion blur from the low-light color images is difficult because the imposed noise hinders accurate motion blur kernel estimation. To overcome this problem, we build a novel imaging system using a single sensor that captures red, green, blue (RGB) and near-infrared (NIR) images. Our imaging system captures low-light scenes with exposure bracketing, which is a technique to acquire multiple images with different exposure times. It thus allows us to obtain the short- and long-exposure RGB/NIR images. Both the short- and long-exposure NIR images taken using an NIR flash unit can be captured with less noise; thus they enable estimation of motion blur kernel accurately. Based on this fact, we perform joint denoising and deblurring of the low-light color image with the estimated motion blur kernel. Our experiments using real raw data captured by our imaging system demonstrate the effectiveness of our method.

***Index Terms*—** low-light image restoration, RGB/NIR single sensor, exposure bracketing, denoising, deblurring

1. INTRODUCTION

The restoration of low-light color images deteriorated with unwanted noise and motion blur is a major subject in the research field of image processing. To reduce such visual artifacts from the captured color images, many methods have been proposed (e.g. denoising [1, 2], deblurring [3–6] etc.). Furthermore, simultaneously capturing color and near-infrared (NIR) images has shown to be effective in restoring low-light color images [7–19]. Because NIR images can be captured with less noise by using an NIR flash unit, they play an important role in effectively eliminating the visual artifacts while preserving the edge details of the scene.

The simultaneous reduction of noise and motion blur from the low-light color images remains difficult. As reported in [20–22], the imposed noises hinder estimating motion blur kernel utilized for removing motion blur from the images.

In this study, we propose a novel imaging system using a single sensor that captures red, green, blue (RGB) and NIR images. Our system captures low-light scenes based on exposure bracketing, which is a technique used to acquire multiple images with different exposure times. Figure 1 shows our imaging system. Our system captures the short- and the long-exposure RGB/NIR images of the low-light scene.

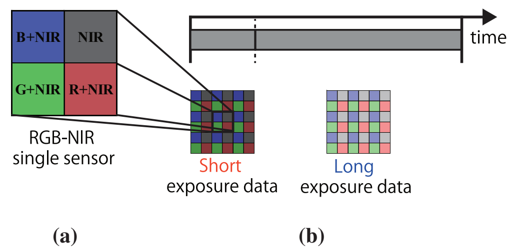

Fig. 1: Proposed imaging system. (a) Color filter array of our RGB/NIR single sensor. (b) Exposure bracketing using our sensor. It enables the acquisition of successive RGB/NIR images taken with the short- and long-exposure times.

Long-exposure imaging is useful in recovering low-light color images as reported in [17]. We also utilize the RGB images captured with the long-exposure time to reconstruct the latent clear color images. However, the long-exposure RGB images are inadequate for estimating motion blur kernel because they include noise. In contrast, the captured NIR images have less noise, thus suggesting that the use of NIR images would enable us to estimate motion blur kernel accurately. We estimate optimal motion blur kernel in the long-exposure NIR images with the help of the motion-blur less NIR images taken with a short-exposure time. As our single sensor enables us to capture RGB and NIR images simultaneously, we can assume that the motion blur kernel estimated using NIR images would be similar to that in the RGB one. Thus, it allows us to perform joint denoising and deblurring of the long-exposure RGB image with reliable motion blur kernel obtained using NIR images.

The main contribution of our work is as follows: 1) We developed a novel imaging system using an RGB/NIR single sensor with exposure bracketing to remove noise and motion blur simultaneously. 2) We proposed an algorithm for jointly denoising and deblurring of low-light color images by using

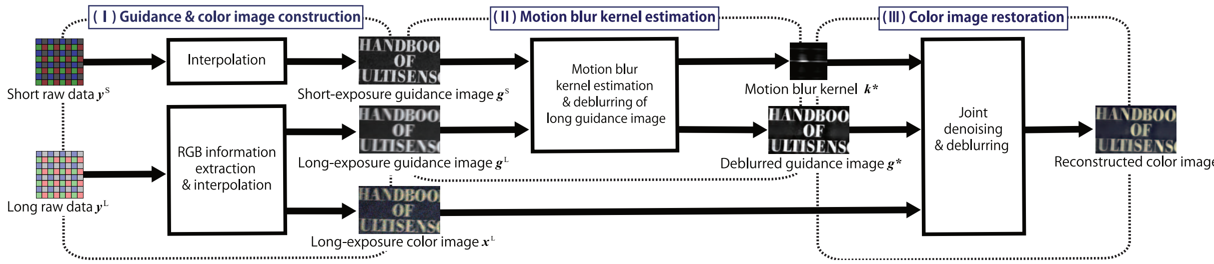

Fig. 2: Overview of our low-light color image restoration. (I) Guidance and color image construction. We interpolate the short- and long-exposure guidance images $\boldsymbol{g}^{\mathrm{S}}$ and $\boldsymbol{g}^{\mathrm{L}}$ by using the previous method [13]. We interpolate long-exposure color image $\boldsymbol{x}^{\mathrm{L}}$ by using a bicubic method, after performing RGB information extraction from $\boldsymbol{y}^{\mathrm{L}}$ [13]. (II) Motion blur kernel estimation. We estimate motion blur kernel $\boldsymbol{k}^*$ using $\boldsymbol{g}^{\mathrm{S}}$ and $\boldsymbol{g}^{\mathrm{L}}$ while exploring the latent deblurred guidance image $\boldsymbol{g}^*$. (III) Color image restoration. We perform joint denoising and deblurring of $\boldsymbol{x}^{\mathrm{L}}$ using $\boldsymbol{k}^*$ and $\boldsymbol{g}^*$.

the short- and long-exposure RGB/NIR images captured using our imaging system. Our algorithm allows us to perform non-blind deblurring of the low-light color image by exploiting the estimated motion blur kernel obtained using the NIR images taken with less noise.

2. OVERVIEW OF PROPOSED METHOD

The goal of this study is to achieve reconstructing noise- and blur-free color images by using the short- and long-exposure RGB/NIR images captured by our imaging system.

Figure 2 provides an overview of our reconstruction scheme. Let the captured raw data taken with the short- and long-exposure times are $\boldsymbol{y}^{\mathrm{S}}$ and $\boldsymbol{y}^{\mathrm{L}}$, respectively. Using $\boldsymbol{y}^{\mathrm{S}}$ and $\boldsymbol{y}^{\mathrm{L}}$, we construct the short- and long-exposure guidance images, $\boldsymbol{g}^{\mathrm{S}}$ and $\boldsymbol{g}^{\mathrm{L}}$, which include NIR information (i.e., less noise) and long-exposure color image $\boldsymbol{x}^{\mathrm{L}}$. In particular, we interpolate $\boldsymbol{g}^{\mathrm{S}}$ and $\boldsymbol{g}^{\mathrm{L}}$ by using previous method [13]. In fact, RGB and NIR information obtained using RGB/NIR single sensor can be separated as reported in [13, 23–25]. We separate the RGB and NIR information by using the method [13]. We then interpolate long-exposure color image $\boldsymbol{x}^{\mathrm{L}}$ by using a bicubic interpolation method. Using noiseless guidance images ($\boldsymbol{g}^{\mathrm{S}}$ and $\boldsymbol{g}^{\mathrm{L}}$), we estimate motion blur kernel. We describe the details of this scheme in Sec. 3. With the estimated motion blur kernel, we jointly perform denoising and deblurring (i.e., non-blind deconvolution) of the color image $\boldsymbol{x}^{\mathrm{L}}$. The details of this processing are described in Sec. 4.

3. MOTION BLUR KERNEL ESTIMATION USING SHORT/LONG GUIDANCE IMAGES

The guidance images $\boldsymbol{g}^{\mathrm{S}}$ and $\boldsymbol{g}^{\mathrm{L}}$ are useful to estimate the motion blur kernel because being with less noise. To estimate optimal motion blur kernel of $\boldsymbol{g}^{\mathrm{L}}$, we exploit short-exposure guidance image $\boldsymbol{g}^{\mathrm{S}}$. The use of an image pair captured with the short- and long-exposure times is effective to estimate motion blur kernel in a long-exposure image [26, 27].

3.1. Observation model

Our scheme jointly estimates the motion blur kernel $\boldsymbol{k}$ as well as the latent clear guidance image. Because our imaging system captures $\boldsymbol{g}^{\mathrm{S}}$ and $\boldsymbol{g}^{\mathrm{L}}$ at the different times, spatial misalignment between them would be observed. In our method, such misalignment would not decrease the accuracy in estimating motion blur kernel because our system based on the exposure bracketing can take the short- and long-exposure images quickly. According to the previous method using multi-shot images [28], such misalignment appears as a shift of the center position of the estimated motion blur kernel. Based on this fact, we model the observation process of $\boldsymbol{g}^{\mathrm{S}}$ and $\boldsymbol{g}^{\mathrm{L}}$ as

$$\begin{aligned} \boldsymbol{g}^{\mathrm{S}} &= \boldsymbol{g} + \boldsymbol{n}^{\mathrm{S}}, \\ \boldsymbol{g}^{\mathrm{L}} &= \boldsymbol{g} \otimes \boldsymbol{k} + \boldsymbol{n}^{\mathrm{L}}, \end{aligned} \tag{1}$$

where $\boldsymbol{g}$, $\boldsymbol{n}^{\mathrm{S}}$, and $\boldsymbol{n}^{\mathrm{L}}$ denote the latent deblurred guidance image, and the imposed noise in the short- and long-exposure guidance image, respectively. In addition, $\otimes$ represents the convolution operator. In the model in Eq. (1), $\boldsymbol{k}$ represents motion blur kernel including the shift caused by the misalignment between $\boldsymbol{g}^{\mathrm{S}}$ and $\boldsymbol{g}^{\mathrm{L}}$. Based on this observation models, we perform an alternating iterative minimization procedure to estimate $\boldsymbol{k}$ and $\boldsymbol{g}$.

3.2. Estimating g

We estimate the latent deblurred guidance image $\boldsymbol{g}$ with the given motion blur kernel $\boldsymbol{k}$ estimated at the previous iteration. We solve the following optimization problem with the control parameters λ_1, λ_2 and λ_3 as,

$$\begin{aligned} \min_{\boldsymbol{g}} \lambda_1 \left|\left|\boldsymbol{g} \otimes \boldsymbol{k} - \boldsymbol{g}^{\mathrm{L}}\right|\right|_2^2 + \lambda_2 \left|\left|\boldsymbol{g} - \boldsymbol{g}^{\mathrm{S}}\right|\right|_2^2 \\ + \lambda_3 \left|\left|\boldsymbol{g} - \mathrm{GIF}\left(\boldsymbol{g}, \boldsymbol{g}^{\mathrm{S}}\right)\right|\right|_2^2 + \left|\left|\bigtriangledown \boldsymbol{g}\right|\right|_p, \end{aligned} \tag{2}$$

where $\mathrm{GIF}\left(\boldsymbol{i}, \boldsymbol{j}\right)$ denotes the operation of guided image filtering [29] with input image $\boldsymbol{i}$ and guidance image $\boldsymbol{j}$. Moreover,

$||\cdot||_p$ denotes ℓ_p norm $(0 < p < 1)$, and $\bigtriangledown$ is the gradient operator. In Eq. (2), the first and the second terms are constraints based on the observation models in Eq. (1), respectively. The third term is a constraint characterizing the fact that $\boldsymbol{g}$ is likely to have the similar structure of the short-exposure guidance image $\boldsymbol{g}^{\mathrm{S}}$ being with less motion blur. The forth term represents a regularization characterizing the fact that the gradients of natural images are drawn from a hyper-Laplacian distribution (i.e., ℓ_p norm representation) as reported in [5].

To solve Eq. (2), we solve the following two subproblems alternately iteratively:

$$\tilde{\boldsymbol{g}} = \mathrm{GIF}\left(\boldsymbol{g}, \boldsymbol{g}^{\mathrm{S}}\right), \tag{3}$$

$$\begin{aligned} \min_{\boldsymbol{g}} \lambda_1 \left|\left|\boldsymbol{g} \otimes \boldsymbol{k} - \boldsymbol{g}^{\mathrm{L}}\right|\right|_2^2 + \lambda_2 \left|\left|\boldsymbol{g} - \boldsymbol{g}^{\mathrm{S}}\right|\right|_2^2 \\ + \lambda_3 \left|\left|\boldsymbol{g} - \tilde{\boldsymbol{g}}\right|\right|_2^2 + \left|\left|\bigtriangledown \boldsymbol{g}\right|\right|_p . \end{aligned} \tag{4}$$

We solve Eq. (3) in the spatial domain using the algorithm proposed in [29], and solve Eq. (4) in the frequency domain using the algorithm proposed in [5]. We iteratively perform the above procedures until the change in $\boldsymbol{g}$ converges.

3.3. Estimating $\boldsymbol{k}$

The salient edges in $\boldsymbol{g}$ are effective in estimating $\boldsymbol{k}$ more accurately, as reported in [4, 16]. Using this fact, we derive $\boldsymbol{k}$ using the estimated $\boldsymbol{g}$ by minimizing the following problem,

$$\min_{\boldsymbol{k}} \lambda_4 \left|\left|\bigtriangledown \hat{\boldsymbol{g}} \otimes \boldsymbol{k} - \bigtriangledown \boldsymbol{g}^{\mathrm{L}}\right|\right|_2^2 + \left|\left|\boldsymbol{k}\right|\right|_p , \tag{5}$$

where $\hat{\boldsymbol{g}}$ is salient edges in $\boldsymbol{g}$ computed by using the method proposed in [4]. The second term characterizes a smoothness constraint for the motion blur kernel $\boldsymbol{k}$ to be estimated. We solve Eq. (5) using iterative re-weighted least squares (IRLS) and conjugate gradient (CG) methods as in [6].

We estimate motion blur kernel in a coarse-to-fine manner by using a multi-scale iterative process as was done in [3, 4, 6, 16]. Finally, we acquire optimal motion blur kernel $\boldsymbol{k}^*$ and optimal guidance image $\boldsymbol{g}^*$.

4. NON-BLIND DEBLURRING OF LOW-LIGHT COLOR IMAGE

We perform non-blind deblurring of the low-light color image $\boldsymbol{x}^{\mathrm{L}}$ with the estimated motion blur kernel $\boldsymbol{k}^*$ and the obtained guidance image $\boldsymbol{g}^*$. Because the short-exposure color image would be heavily deteriorated by noise, we estimate $\boldsymbol{x}$ by using $\boldsymbol{x}^{\mathrm{L}}$. We solve the following optimization problem,

$$\begin{aligned} \min_{\boldsymbol{x}} \omega_1 \left|\left|\boldsymbol{x} \otimes \boldsymbol{k}^* - \boldsymbol{x}^{\mathrm{L}}\right|\right|_2^2 \\ + \omega_2 \left|\left|\boldsymbol{x} - \mathrm{GIF}\left(\boldsymbol{x}, \boldsymbol{g}^*\right)\right|\right|_2^2 + \left|\left|\bigtriangledown \boldsymbol{x}\right|\right|_p , \end{aligned} \tag{6}$$

where ω_1 and ω_2 are control parameters. In Eq. (6), the second term based on a guided image filtering contributes to reducing the noise of the color image to be recovered. We solve Eq. (6) using the similar manner as that for solving Eq. (2).

5. EXPERIMENTS

We present experimental results to demonstrate the effectiveness of our method using raw data captured by our imaging system. In this experiment, we set the short- and long-exposure time to 5.01 ms, 33.0 ms, respectively. We tested our system using 20 real raw data. We considered two examples of our restoration results in this paper. We conducted preliminary experiments for finding optimal parameters using raw data different from those used in testing. After that, we set control parameters for our image restoration to $p = 0.8, \lambda_1 = 200, \lambda_2 = 100, \lambda_3 = 200, \lambda_4 = 1, \omega_1 = 200, \omega_2 = 700$. We used the same parameters for all the experiments.

In fact, it is hard to directly compare other state-of-the-art methods because our imaging system differs from that of previous methods. However, the performance of color image restoration processing itself can be able to be evaluated if we assumed that the input color and guidance images are given. In this condition, we compared state-of-the-art methods that perform joint denoising and deblurring of color image taken in low-light scenes. We set parameters of each method to be such that it could output the best qualitative results.

We first compared state-of-the-art method [22] that performs joint denoising and deblurring of single color image. We used $\boldsymbol{x}^{\mathrm{L}}$ as the input image for this method. Figure 3 shows the reconstruction results for a low-light scene. The input color image $\boldsymbol{x}^{\mathrm{L}}$ is shown in Fig. 3(a). We can see that $\boldsymbol{x}^{\mathrm{L}}$ includes both noise and motion blur. The captured short- and long-exposure guidance images $\boldsymbol{g}^{\mathrm{S}}$ and $\boldsymbol{g}^{\mathrm{L}}$ are shown in Figs. 3(b) and (c), respectively. Figure 3(d) shows the deblurred guidance image $\boldsymbol{g}^*$ and the estimated motion blur kernel $\boldsymbol{k}^*$ (shown in the white rectangle at the upper left in Fig. 3(d)) obtained by using our method. We can qualitatively see that our method could perform deblurring of the long-exposure guidance image. Figures 3(e) and 3(f) show the reconstruction results obtained using the method [22] and our method, respectively. We can see that our method showed better performance in restoring the low-light color image than the method [22].

We conducted further comparison experiments. We compared our method with other state-of-the-art methods for color image restoration with the help of the guidance image. We used two methods [10, 16] that perform joint denoising and deblurring of color image by exploiting a guidance image. We used $\boldsymbol{x}^{\mathrm{L}}$ and $\boldsymbol{g}^*$ as the input images for these methods [10, 16]. We note that Seo's method [10] performed color image restoration without estimating the motion blur kernel.

Figure 4(a) shows the short-exposure color image taken by our imaging system (Note that not all methods use this, just for reference.). We can see that this short-exposure color image was heavily deteriorated by noise. Further, Figs. 4(b)-(d) show the input images used in our method. Fig. 4(e) show the deblurred guidance image and the estimated motion blur kernel obtained using our method. Figs. 4(f)-(h) show reconstruction results obtained using the methods [10, 16], and

(a) Captured $\boldsymbol{x}^{\mathrm{L}}$ **(b)** Captured $\boldsymbol{g}^{\mathrm{S}}$

(c) Captured $\boldsymbol{g}^{\mathrm{L}}$ **(d)** Reconstructed $\boldsymbol{g}^{*}$

(e) Result of [22] **(f)** Our result

Fig. 3: Comparison results in low-light color image restoration with the method [22]. The estimated motion blur kernels obtained using our method and the method [22] are shown in the upper left (white rectangular images) in (d) and (e), respectively. The motion blur kernel is of size 61×61.

our method, respectively. As shown in Fig. 4(f), the motion blur kernel estimation using color image was difficult even for state-of-the-art method [16] owing to heavy noise. In contrast to the method [16], our motion blur kernel estimation using the guidance images ($\boldsymbol{g}^{\mathrm{S}}$ and $\boldsymbol{g}^{\mathrm{L}}$) can be performed with less effect of noise (Fig. 4(e)). Moreover, we can also see that our method showed better restoration result than those obtained using the methods [10, 16]. This comparison evaluation clearly showed that our method is effective for color image restoration.

6. CONCLUSION

We proposed a novel imaging system using an RGB/NIR single sensor with exposure bracketing to simultaneously remove motion blur and noise of low-light color images. We proposed an algorithm for jointly denoising and deblurring of low-light color images by using the short- and long-exposure RGB/NIR images captured using our imaging system. Our algorithm allows us to perform non-blind deblurring of the low-light color image by exploiting the estimated motion blur kernel obtained using the short- and long-exposure NIR images taken with less noise. Through the experiments using real raw data captured by our imaging system, we demonstrated that our method reconstructed clear color images better than those obtained using state-of-the art methods.

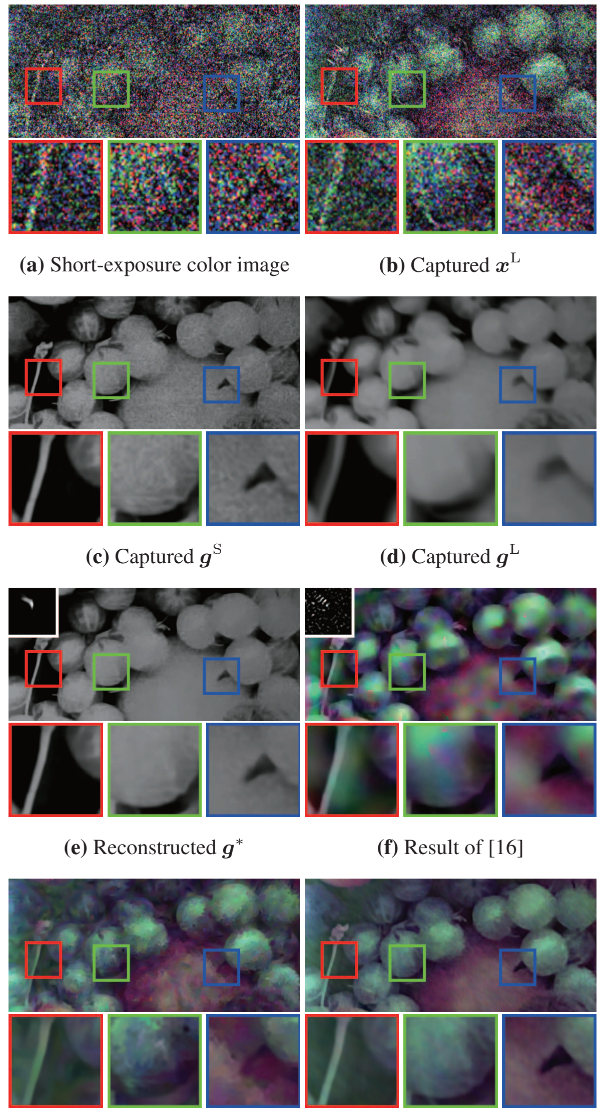

(a) Short-exposure color image **(b)** Captured $\boldsymbol{x}^{\mathrm{L}}$

(c) Captured $\boldsymbol{g}^{\mathrm{S}}$ **(d)** Captured $\boldsymbol{g}^{\mathrm{L}}$

(e) Reconstructed $\boldsymbol{g}^{*}$ **(f)** Result of [16]

(g) Result of [10] **(h)** Our result

Fig. 4: Comparison results in low-light color image restoration with the methods [10, 16]. These comparison methods utilized $\boldsymbol{g}^{*}$ as the guidance image for deblurring of $\boldsymbol{x}^{\mathrm{L}}$. The estimated motion blur kernels using our method and the method [16] are shown in upper left in (e) and (f), respectively. The motion blur kernel is of size 55×55.

Acknowledgment This work described in this paper was partially supported by SHARP Corporation.

7. REFERENCES

[1] A. Buades and B. Coll, "A non-local algorithm for image denoising," in *IEEE CVPR*, 2005, pp. 60–65.

[2] K. Dabov, A. Foi, V. Katkovnik, and K. Egiazarian, "Image denoising by sparse 3-D transform-domain collaborative filtering," *IEEE TIP*, vol. 16, no. 8, pp. 2080–2095, 2007.

[3] R. Fergus, B. Singh, A. Hertzmann, S. T. Roweis, and W. T. Freeman, "Removing camera shake from a single photograph," *ACM TOG*, vol. 25, pp. 787–794, 2006.

[4] S. Cho and S. Lee, "Fast motion deblurring," *ACM TOG*, vol. 28, no. 5, p. 145, 2009.

[5] D. Krishnan and R. Fergus, "Fast image deconvolution using hyper-laplacian priors," in *NIPS*, 2009, pp. 1033–1041.

[6] D. Krishnan, T. Tay, and R. Fergus, "Blind deconvolution using a normalized sparsity measure," in *IEEE CVPR*, 2011, pp. 233–240.

[7] E. P. Bennett, J. L. Mason, and L. McMillan, "Multispectral bilateral video fusion," *IEEE TIP*, vol. 16, no. 5, pp. 1185–1194, 2007.

[8] D. Krishnan and R. Fergus, "Dark flash photography," *ACM TOG*, vol. 28, no. 3, 2009.

[9] S. Zhuo, X. Zhang, X. Miao, and T. Sim, "Enhancing low light images using near infrared flash images," in *IEEE ICIP*, 2010, pp. 2537–2540.

[10] H.-J. Seo and P. Milanfar, "Robust flash denoising/deblurring by iterative guided filtering," *EURASIP J. Adv. Sig. Process.*, vol. 2012, no. 1, pp. 1–19, 2012.

[11] Q. Yan, X. Shen, L. Xu, S. Zhuo, X. Zhang, L. Shen, and J. Jia, "Cross-field joint image restoration via scale map," in *IEEE ICCV*, 2013, pp. 1537–1544.

[12] H. Honda, R. Timofte, and L. Van Gool, "Make my day - high-fidelity color denoising with near-infrared," in *IEEE PBVS*, 2015.

[13] H. Yamashita, D. Sugimura, and T. Hamamoto, "Enahancing low-light color image using an RGB-NIR single sensor," in *IEEE VCIP*, 2015, pp. 119–121.

[14] T. Shibata, M. Tanaka, and M. Okutomi, "Versatile visible and near-infrared image fusion based on high visibility area selection," *J. Electron. Imaging.*, vol. 25, no. 1 013016, 2016.

[15] C.-H. Son and X.-P. Zhang, "Layer-based approach for image pair fusion," *IEEE TIP*, vol. 25, no. 6, pp. 2866–2881, 2016.

[16] W. Li, J. Zhang, and Q.-H. Dai, "Robust blind motion deblurring using near-infrared flash image," *J. Vis. Commun. and Image Represent.*, vol. 24, no. 8, pp. 1394–1413, 2013.

[17] D. Sugimura, T. Mikami, H. Yamashita, and T. Hamamoto, "Enhancing color images of extremely low light scenes based on RGB/NIR images acquisition with different exposure times," *IEEE TIP*, vol. 24, no. 11, pp. 3586–3597, 2015.

[18] S. Matsui, T. Okabe, M. Shimano, and Y. Sato, "Image enhancement of low-light scenes with near-infrared flash images," in *ACCV*, 2009, pp. 213–223.

[19] T. Yue, M.-T. Sun, Z. Zhang, J. Suo, and Q. Dai, "Deblur a blurred RGB image with a sharp NIR image through local linear mapping," in *IEEE ICME*, 2014, pp. 1–6.

[20] N. Joshi, C. L. Zitnick, R. Szeliski, and D. J. Kriegman, "Image deblurring and denoising using color priors," in *IEEE CVPR*, 2009, pp. 1550–1557.

[21] Y.-W. Tai and S. Lin, "Motion-aware noise filtering for deblurring of noisy and blurry images," in *IEEE CVPR*, 2012, pp. 17–24.

[22] L. Zhong, S. Cho, D. Metaxas, S. Paris, and J. Wang, "Handling noise in single image deblurring using directional filters," in *IEEE CVPR*, 2013, pp. 612–619.

[23] Z. Chen, X. Wang, and R. Liang, "RGB-NIR multispectral camera," *Opt. Express*, vol. 22, no. 5, pp. 4985–4994, 2014.

[24] H. Tang, X. Zhang, S. Zhuo, F. Chen, K. N. Kutulakos, and L. Shen, "High resolution photography with an RGB-infrared camera," in *IEEE ICCP*, 2015, pp. 1–10.

[25] M. Martinello, A. Wajs, S. Quan, H. Lee, C. Lim, T. Woo, W. Lee, S. S. Kim, and D. Lee, "Dual aperture photography: Image and depth from a mobile camera," in *IEEE ICCP*, 2015, pp. 1–10.

[26] L. Yuan, J. Sun, L. Quan, and H.-Y. Shum, "Image deblurring with blurred/noisy image pairs," *ACM TOG*, vol. 26, no. 3, p. 1, 2007.

[27] H. Zhang, D. Wipf, and Y. Zhang, "Multi-observation blind deconvolution with an adaptive sparse prior," *IEEE TPAMI*, vol. 36, no. 8, pp. 1628–1643, 2014.

[28] S. Zhuo, D. Guo, and T. Sim, "Robust flash deblurring," in *IEEE CVPR*, 2010, pp. 2440–2447.

[29] K. He, J. Sun, and X. Tang, "Guided image filtering," *IEEE TPAMI*, vol. 35, no. 6, pp. 1397–1409, 2013.